Chapter 4. Results and Discussion

4.1 Results of heat treatment process

4.1.1 Heat treatment with different temperatures

After the cleaning process, we put the Ni 150Å, Au 50Å substrate into the thermal furnace. The substrates after heat treatment with different temperature would lead to different morphology. Figure 4.1 shows that with temperature range 500℃~780℃ the surface roughness seems to increase as temperature increasing. This might result to more violent inter-diffusion between nickel and gold layer. As temperature goes up to 780℃ above, the nano-particles which mostly contain nickel and gold were produced. Until 1000℃, we could see a large amounts of jellyfish-like nanostructures being produced.

4.1.2 Analysis of jellyfish-like nanostructure

Figure 4.2 shows the image of the jellyfish-like nanostructure under scanning electron microscopy (SEM). From Fig. 4.2 (b), we could see that the wires were protruded out of the head-like particles. It was for sure that head-like particles are the growing source of the feet-like wires. The energy dispersive X-ray spectroscope (EDS) within SEM shows the particles contain nickel, gold, silicon and oxygen. The bottom ground not surprisingly is silicon oxide. In order to analyze the composition and structure of the nano-wires, we use transmission electron microscopy (TEM) with EDS to identify them. Figure 4.3 exhibits the obvious electron contrast between wires and particles. TEM observations and electron diffraction analyses revealed that all nanowires are amorphous and homogeneous without any crystalline domains. Several elements are detected through EDS such as silicon, oxygen, copper and carbon. The copper signal is attributed to the base holder of copper grid and the

carbon originate from the carbon film spread between copper grid. Surface Auger microscopy (SAM) were also used to speculate the composition of the jellyfish-like nanostructure. Figure 4.4 shows the three detected points on substrate. Especially from the silicon peak in the spectrum, the *R* peak was definitely lower than *L* one. So it meant that the silicon is bonded to another element according to SAM handbook. This totally fitted in with the result from TEM analysis that the nanowires were formed by amorphous silicon oxide.

4.1.3 Heat treatment of dual metal layer with different thickness

In order to identify the relation of metal and silicon oxide nanowires, we coated the dual metal layer with different thickness. Figure 4.5 shows that as gold thickness is increased to 130Å, the existence of head-like particles seem to be vanished because of the growth of nanowires. From this result, the higher atomic percentage of gold profits the growth of silicon oxide nanowires comparing to nickel. The trend is that the length of wires is increased due to the composition percentage increased of gold.

4.1.4 Heat treatment with different cooling rates

With the treatment under different cooling rate, the number of nanowires seems to be the largest amount in the range of properly cooling rate. Figure 4.6 shows that too fast or slow cooling result in the reduction of nanowires quantity. In our experiments, the cooling rate around 1.4℃/sec was the one that protrudes the most nanowires. When the cooling rate went so slow as 0.2℃/sec, the production of silicon oxide nanowires becomes difficult that barely no nanowires spotted.

4.2 Discussion to the growth of nanowires

Recently there are several researches in the characteristics of synthesizing silicon or silicon oxide nanowires [47~52]. Various methods have been developed for synthesizing silicon oxide nanowires including simply heating silicon wafers to high temperature [53~55] and the thermal evaporation of silicon-based powders in the presence of catalysts such as Au and transition metals [56~61]. Recently, Pan et al. [62] and Zheng et al. [63] reported the growth of highly aligned silicon oxide nanowires by using molten Ga as the catalyst and a silicon wafer as the silicon source via a vapor-liquid-solid (VLS) process [64, 65].

In our experiments we observed the results of a batch of amorphous silicon oxide nanowires protruding from the lower hemisphere of the alloy ball whose composition is mixture of gold, nickel, silicon and oxygen elements. The shape of jellyfish-like nanostructure in our experiment is very familiar to the results of ref. [66]. The growth of silicon oxide nanowires might be a process that is analogous to the solution-liquid-solid (SLS) mechanism [67]. The source of silicon oxide should originate from dissolving of amorphous silicon oxide layer below the gold and nickel layers because of the high temperature as 1000℃. For the heat treatment increased to 1000℃ the nickel and gold layers would melt to small silicon oxide-containing balls and the silicon oxide nanoparticles would form on the lower hemisphere surface of alloy ball until reaching supersaturation. These particles acted as nucleating sites and initiate the growth of a batch of silicon oxide nanowires. The alloy ball is then pushed away from the substrate by the growing nanowires. When the force is large enough, the alloy balls would be lifted upward. Gradually, the jellyfish-like nanostructures are formed uniformly distributed on the substrate with white-colored by naked eye.

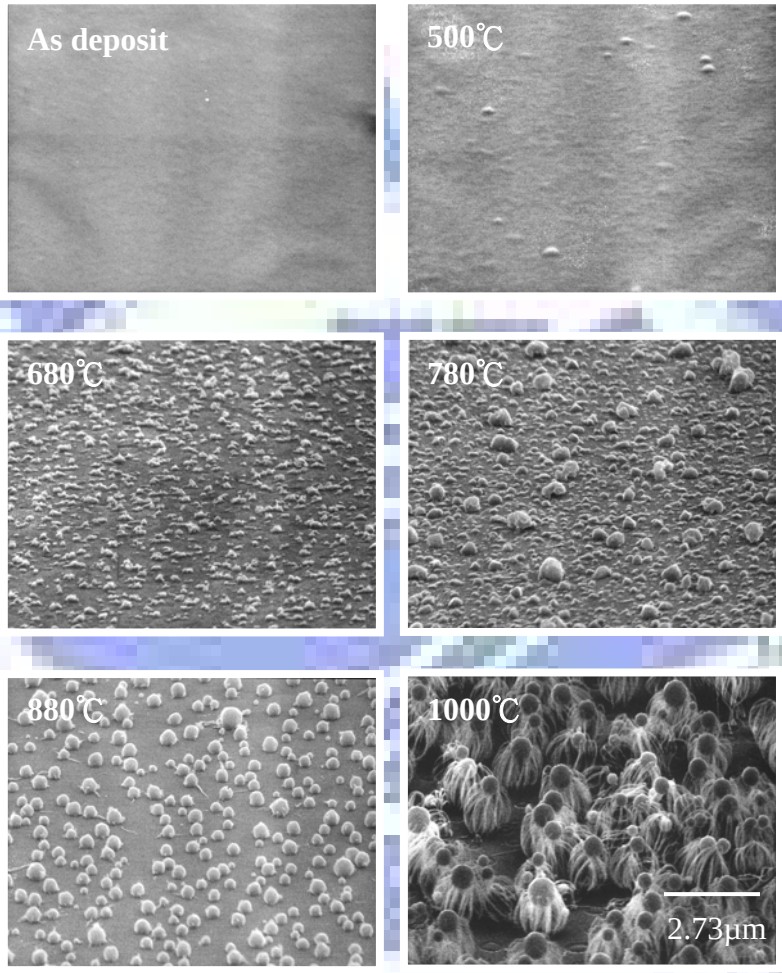

Fig. 4.1 The SEM images of substrates after different temperature heat treatment

Ni 150Å　Au 50Å　　Maintain 2 hrs　　Cooling rate　2℃/sec

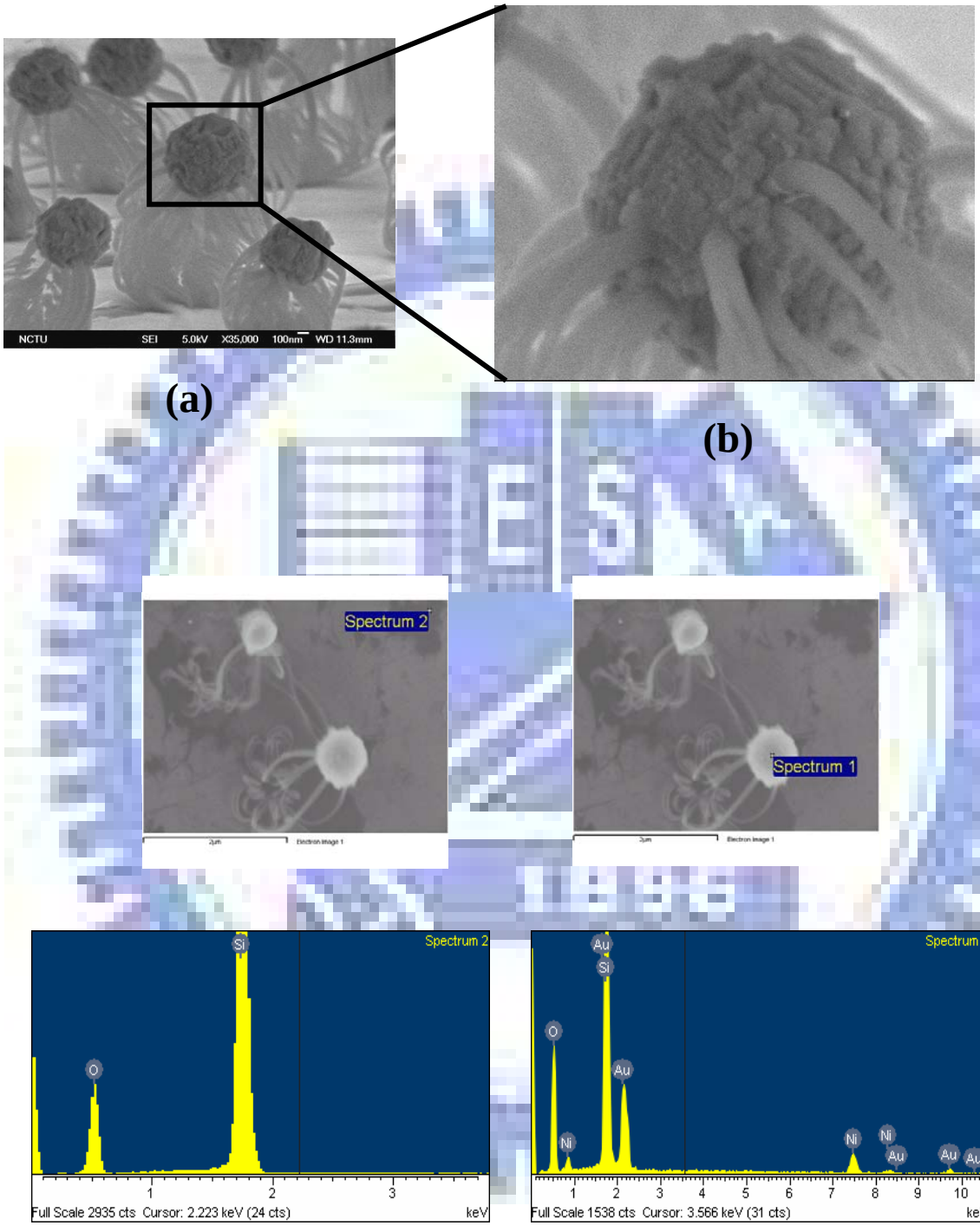

Fig. 4.2 (a) SEM image of jellyfish-like nanostructure with low magnitude (b) SEM image with high magnitude (c) SEM EDS analysis of jellyfish-like nanostructure

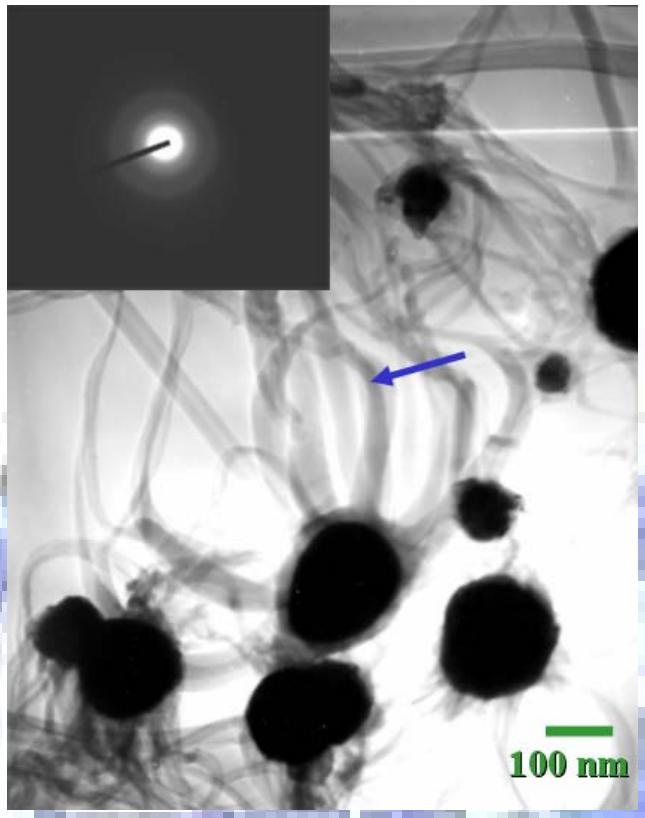

(a)

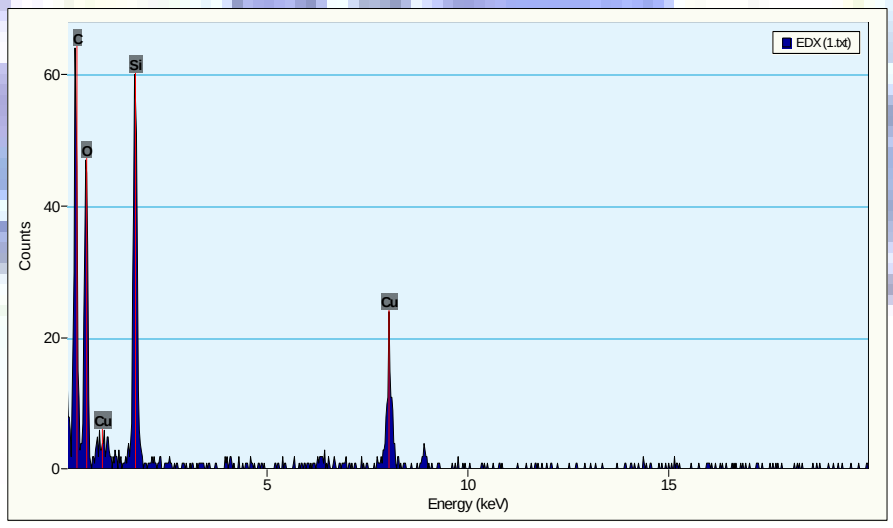

(b)

Fig. 4.3 (a) TEM image of jellyfish-like nanostructure (b) TEM EDS analysis

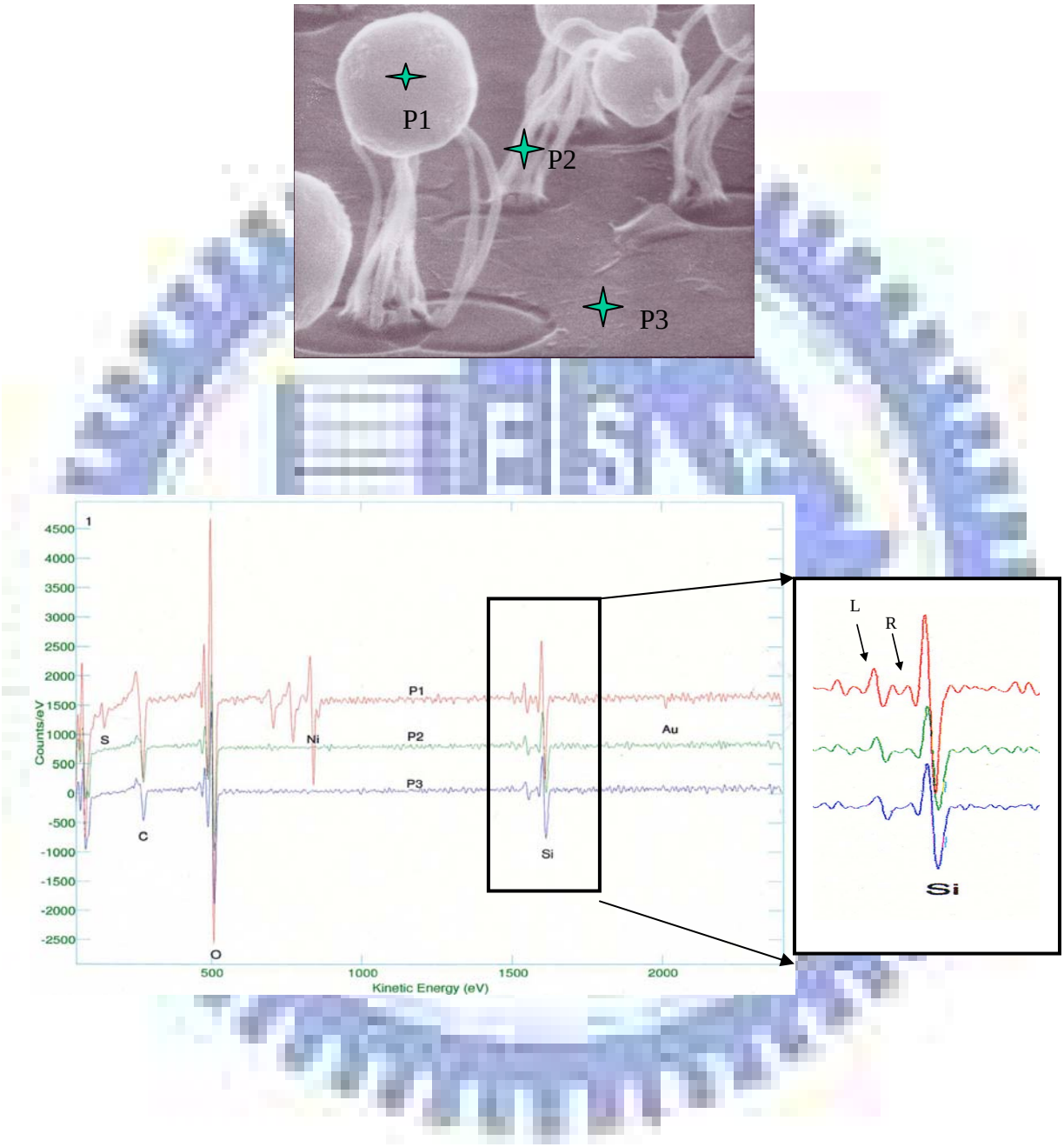

Fig. 4.4 Analysis of jellyfish-like nanostructure with Surface Auger Microscopy

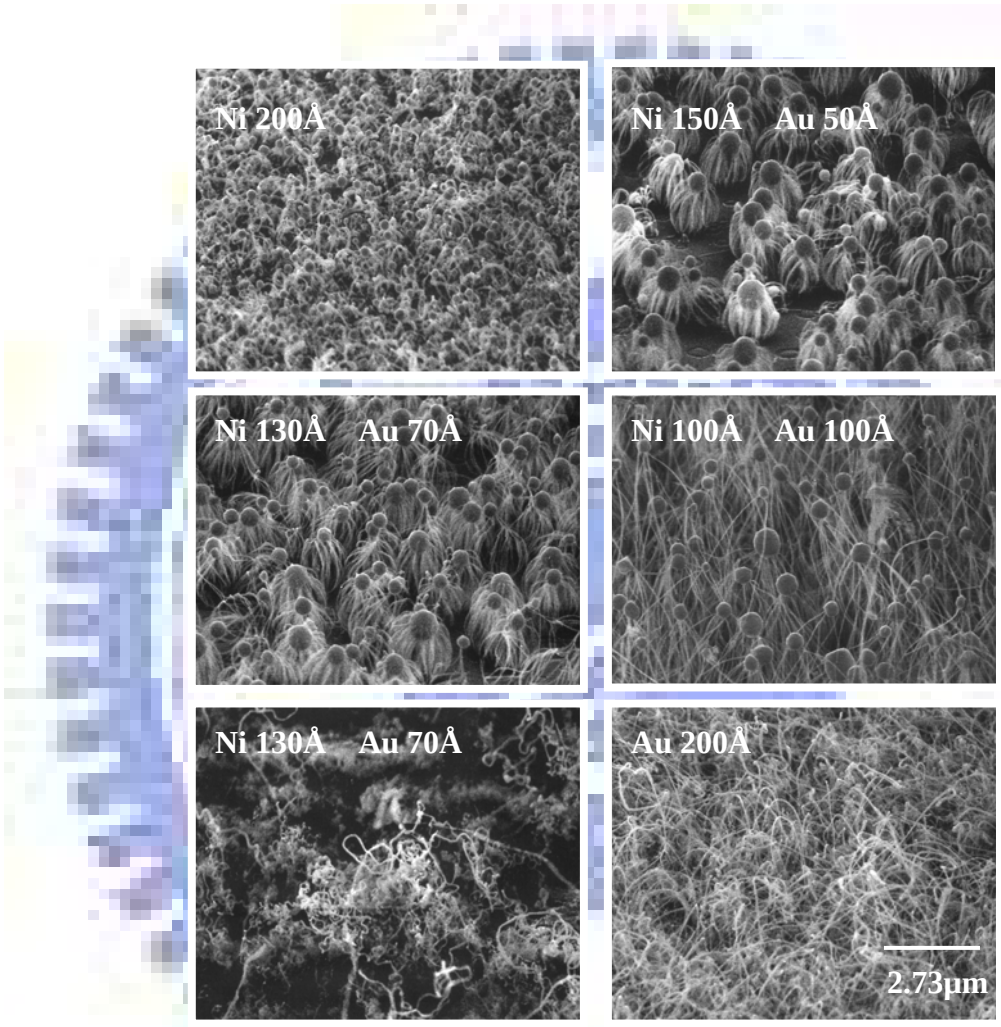

Fig. 4.5 Heat treatment with different metal layer thickness

1000℃ Maintain 2 hrs Cooling rate 2 ℃/sec

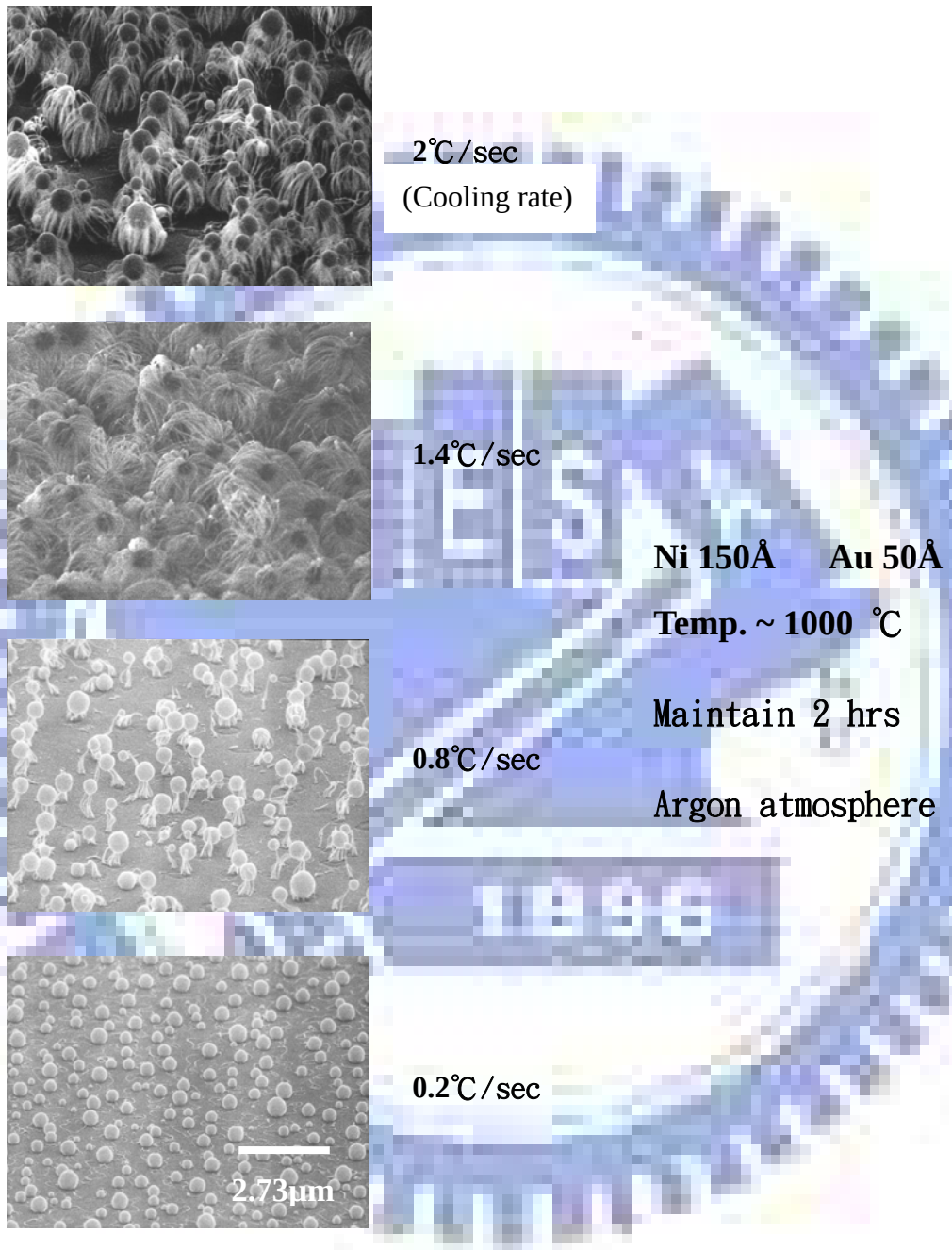

Fig. 4.6 Heat treatment with different cooling rate

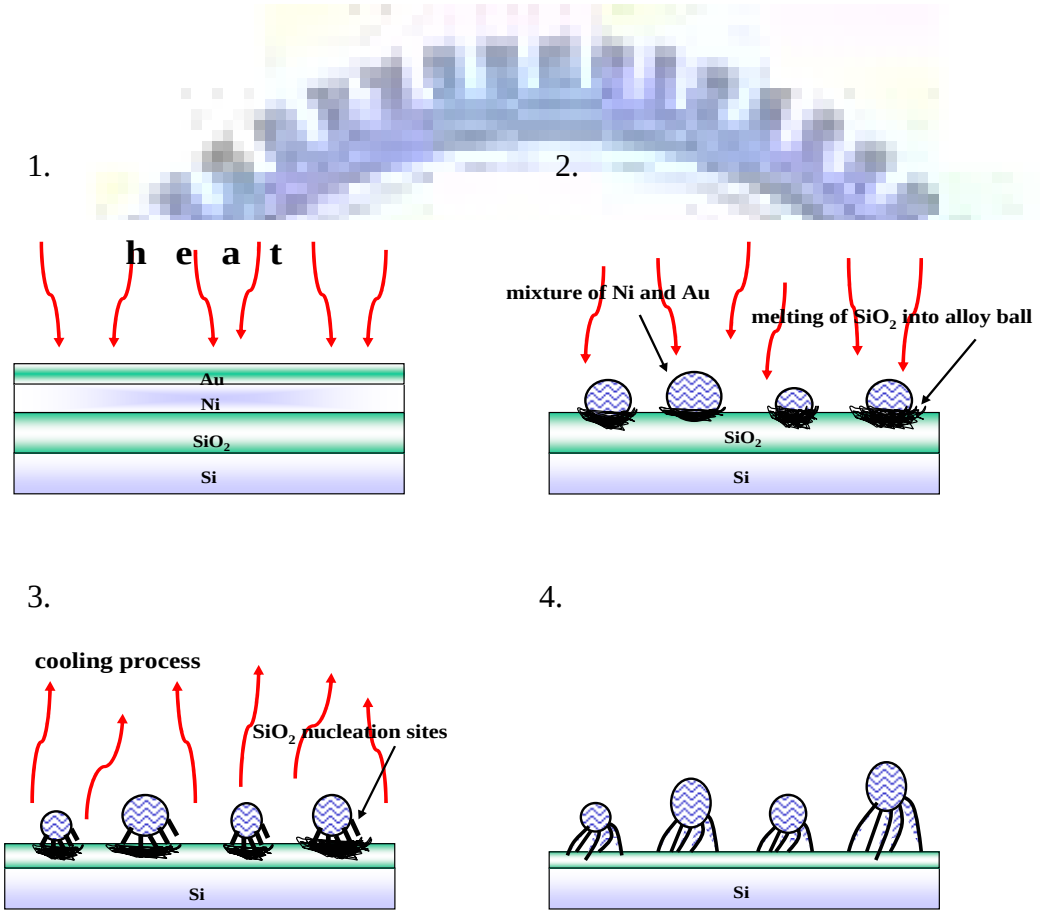

Fig. 4.7 The growth steps of jellyfish-like nanostructure

4.3 Results of the carbon nanotubes growth

4.3.1 Growth of CNTs from different temperature treated substrate

After the heat treatment at different temperatures, we took the substrates with all kinds of morphology to grow carbon nanotubes *via* microwave plasma chemical vapor deposition system. The substrate after 1000℃ heat treatment would grow carbon nanotubes with discontinuous distribution and well alignment. The site density of CNTs is around 6.1 x 10^7 cm^{-2} and this should meet the needs for us to reduce the density of CNTs. The aligned CNTs grew around the rod-like carbide structure about 6 micro-meter height and sites between the rod-like structures would grow aligned CNTs with relatively ultra-short height. From Fig. 4.7, it is interesting that the CNTs growing from substrates below 1000℃ heat treatment appears to be curved ones. As the treatment temperature increased, the number of curved CNTs decreases. The reason why that the quantity of curved CNTs would decrease as treatment temperature increased should relate to the reductant role of H_2 plasma which reduces the nickel oxide into nickel. The amount of nickel oxide might increase with the higher temperature treatment. So the amount of nickel oxide being transformed to nickel should be also increased and finally resulted to larger amounts of straight CNTs. Figure 4.9 shows the raman shift measuring of the substrates at 500℃, 680℃, and 780℃. According to the calculating of I_D/I_G, the value was slightly increased as the temperature decreased, which means that the curved CNTs contained more defects. The TEM analyses are shown as Fig. 4.10 and Fig. 4.11. Comparing these analyses, the catalyst for growing curved CNTs is apparently consisted of gold which may result in heptagon and pentagon carbon structures in graphite sheets. Existing of heptagon and pentagon which replace hexagon should cause the bending or twisting of carbon nanotubes.

4.3.2 Growth of CNTs with different density

In the previous results, the growth of discontinuous distributed CNTs seems to have relationship with jellyfish-like nanostructures. The CNTs grown with different metal layer thickness substrates are shown in Fig. 4.12. The growth condition is fixed to all specimens. It was inspired to find that substrates with (Ni 150Å / Au 50Å, Ni 130Å / Au 70Å, Ni 100Å / Au 100Å) are produced of different density of discontinuous distributed CNTs. At the high temperature as 1000℃, there was a great probability of the formation of nickel silicide and nickel oxide during heat treatment process with pure nickel. But Si-O bond (798 kJ/mol) is stronger than Ni-O bond (391.6 kJ/mol) [70], so nickel oxide should exist with a relatively small amount. Substrate with pure nickel can not grow CNTs and the growth products seem to be rod-like nanoparticles due to the disability of hydrogen plasma which served as reductant to transform nickel silicide into nickel. The Au-Si bond (312 kJ/mol) is slightly lower than Ni-Si bond (318 kJ/mol), so gold would serve as a competitor to nickel for forming silicide. As the gold thickness increasing to 130Å the aligned CNTs are translated to cylindrical-shaped nanorod. The substrate with pure gold would result in amorphous carbon film.

4.4 The explanations to the growth of density reduced CNTs

According to the experiment results, we could find that the octopus-like nanostructure have a close relation to the growth of density-reduced carbon nanotubes. The aligned carbon nanotubes were observed to grow around the rod-like nanostructures which may be the carbide compounds or carbon-covered particles forming by head part of jellyfish-like nanostructures. We speculated the growth of density-reduced CNTs in Fig. 4.13. First, the jellyfish-like nanostructures are exposed under the atmosphere of methane and hydrogen plasma with a bias of -150 V being applied which attracts the plasma to flow downward more frequently. Second, the feet part of silicon oxide nanowires are hit and etched mainly by hydrogen plasma that breaks the linkage between alloy balls and nanowires. The alloy balls were fallen down to the surface of substrate. Third, some of the nickel oxide which distributed near the surface of alloy balls would be transformed into nickel. The hydrogen plasma served as the reductant in this process. A small amount of nickel near the surface of alloy ball might etch away and evaporated to the place between alloy balls that cause the growth of short and sparse CNTs. Fourth, the carbon source which came from the methane plasma would deposit and dissolve into the liquid-phase nickel near the surface of molten-type alloy balls. The carbon are continuously fed into liquid-phase nickel and also the other parts of molten-type alloy balls. Carbon catalyzed by the nickel near the surface of alloy ball would form aligned CNTs around the rod-like nanostructure. The formation of rod-like nanostructure should result to the lack of catalysis ability for growing CNTs to the compounds such as nickel silicide, gold silicide and silicon oxide in the alloy balls. The continuously fed carbon might cover as amorphous carbon film onto the surface of alloy balls and gradually form structures like rod. As the atomic percent of nickel in alloy balls was decreased due to the decrement of nickel thickness, the density of CNTs was simultaneously decreased.

4.5 Field emission measurement from different density of CNTs

According to the articles (see ref. [16] [17] [18]) reported before, the field emission property of discontinuous distributed CNTs should be enhanced due to the screening effect. Since we have grown CNTs with reduction to its density, the relationship between field emission property and density of carbon nanotubes should be verified. The field emission property of the continuous CNT film grown by pure nickel substrate without heat treatment whose density is around 2.2 x 10^8 cm^{-2} was measured comparing to the ones that we have grown with density 6.1 x 10^7 cm^{-2}, 4.7 x 10^7 cm^{-2} and 3.3 x 10^7 cm^{-2}. Figure 4.14 & 4.15 respectively show the bird-eye view and cross-section view of the four emission samples with different CNT density. From the cross-section image, it is clear to see that the height of four samples is nearly equal to 6 μm. The field emission result shown in Fig. 4.16 demonstrates that for decreasing density of CNT the turn-on voltage is decreased. The lowest turn-on voltage which comes from the lowest CNT density is about 2.2 V/μm. It is a great improvement comparing to turn-on voltage of continuous CNT film which is 5.5 V/μm. The value measured from the field emission was sent to fit into the Fowler-Nordheim equation. Figure 4.17 shows that the field emission properties of four emission samples are well obeyed to the Fowler-Nordheim equation. Four traditional F-N plots are observed and the transition of the plot which means the transformation of conductive CNT to semi-conductive one is also observed. Depending on the plot we drawn in Fig. 4.18, the field emission enhancement factor is increased as the density of CNTs decreased. The values of enhancement factor would be 2386, 2218, 2100, and 1910, respectively.

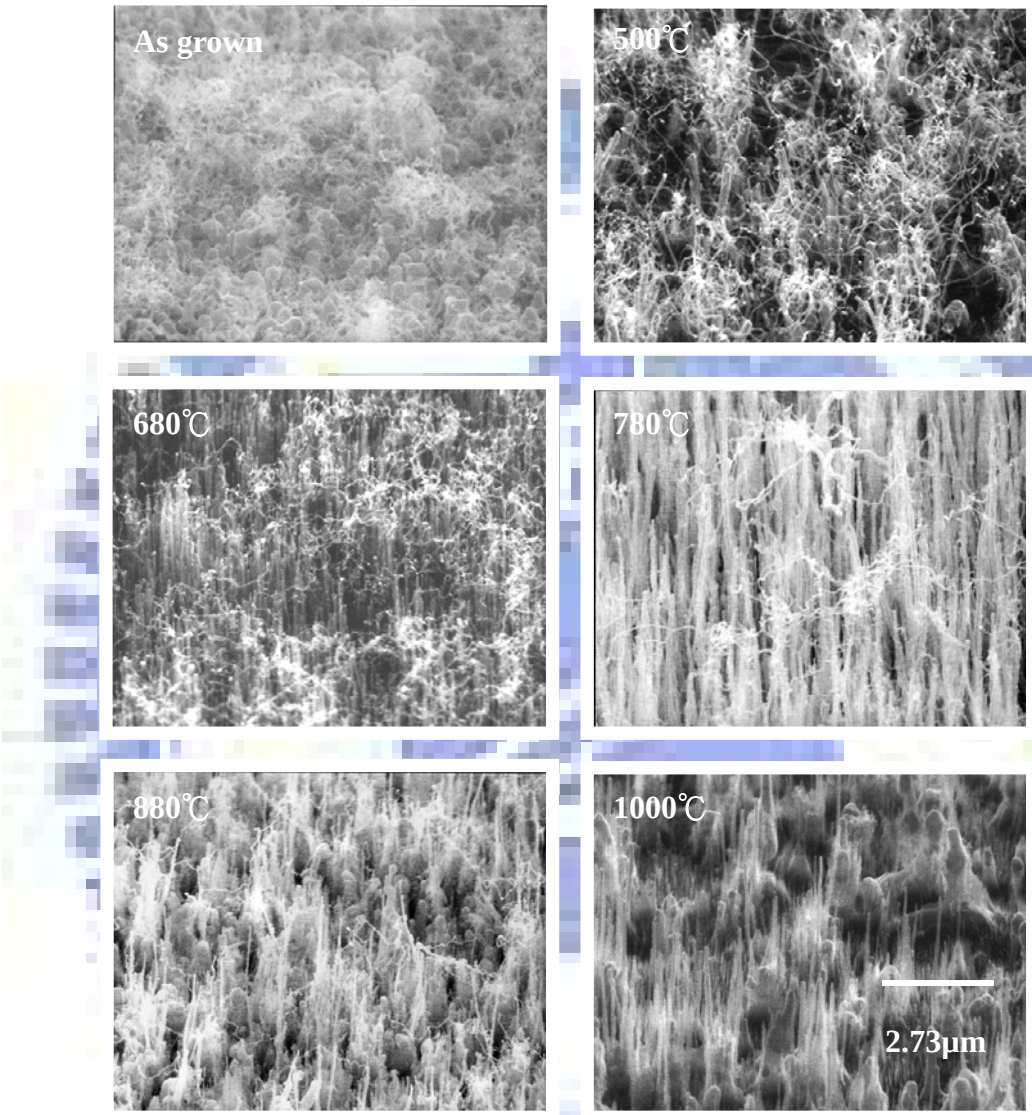

Fig. 4.8 Growth of CNTs from different temperature treated substrate

CH_4 10 sccm H_2 40 sccm 400W -150V 10min 15torr

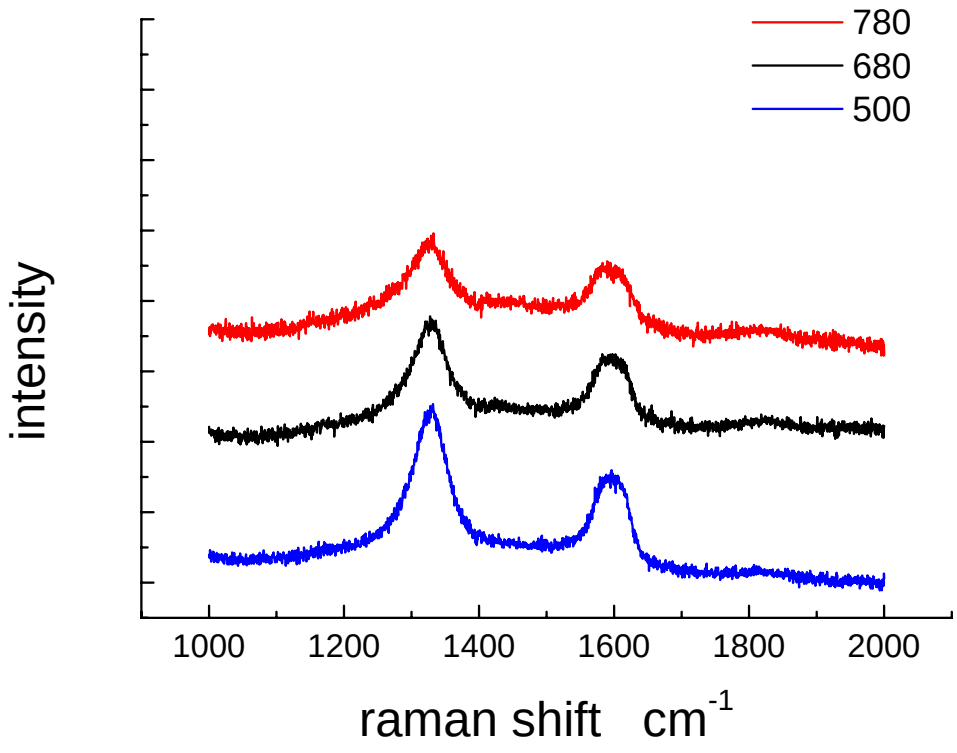

	500℃	680℃	780℃
I_D/I_G	2.19	2.12	1.51

Fig. 4.9 Raman shift measurement

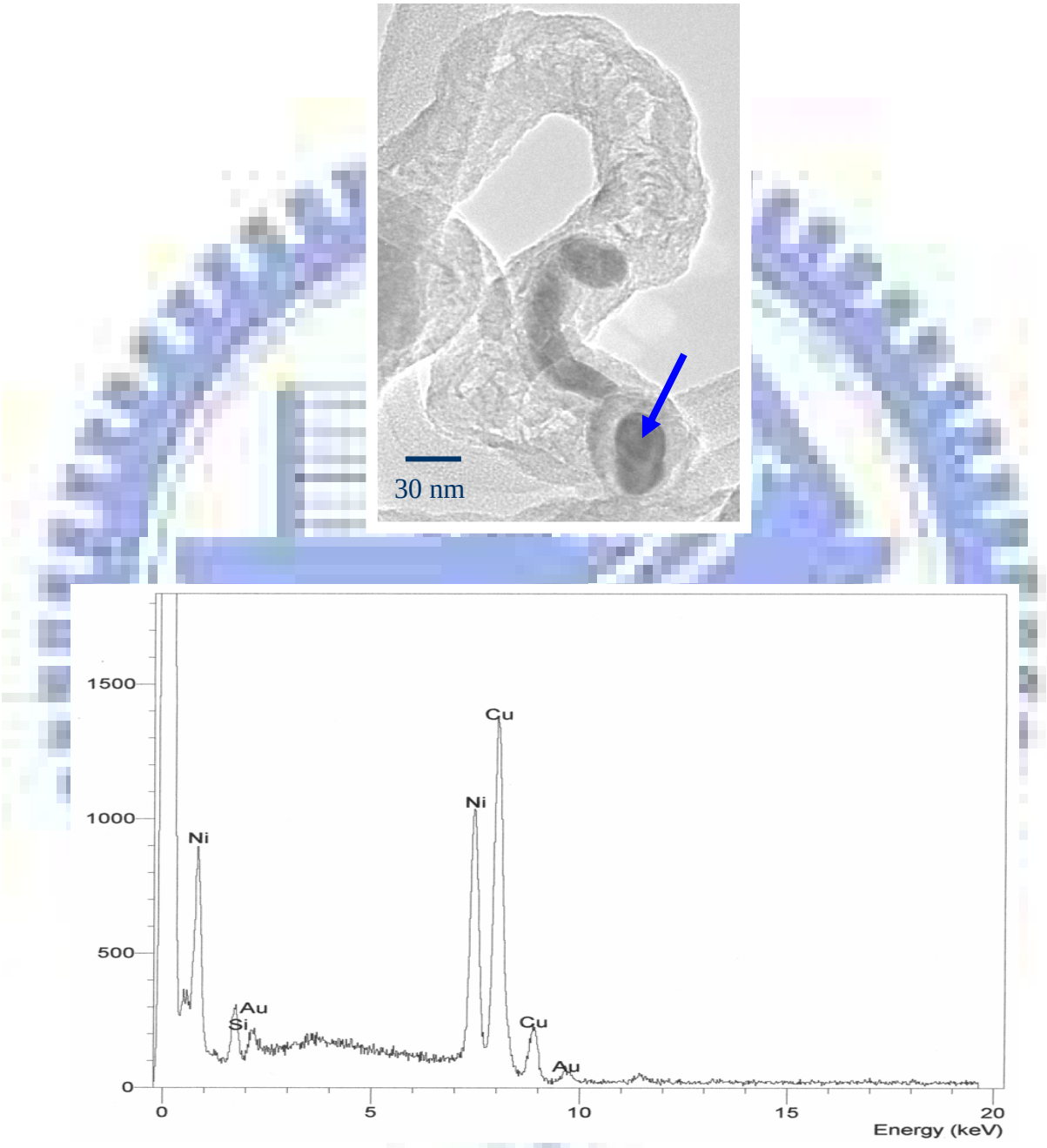

Fig. 4.10 TEM with EDS analysis of the curved carbon nanotubes

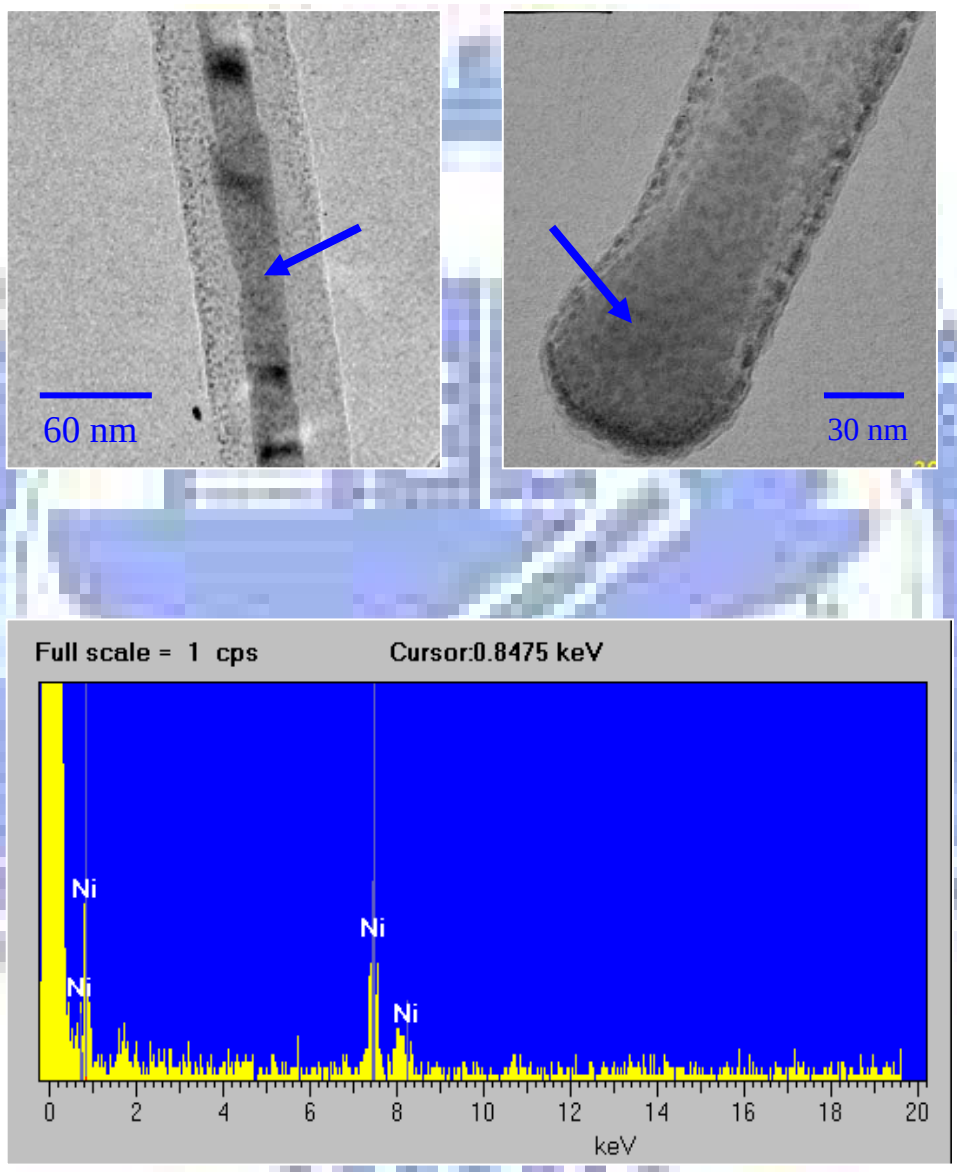

Fig. 4.11 TEM with EDS analysis of the straight carbon nanotubes

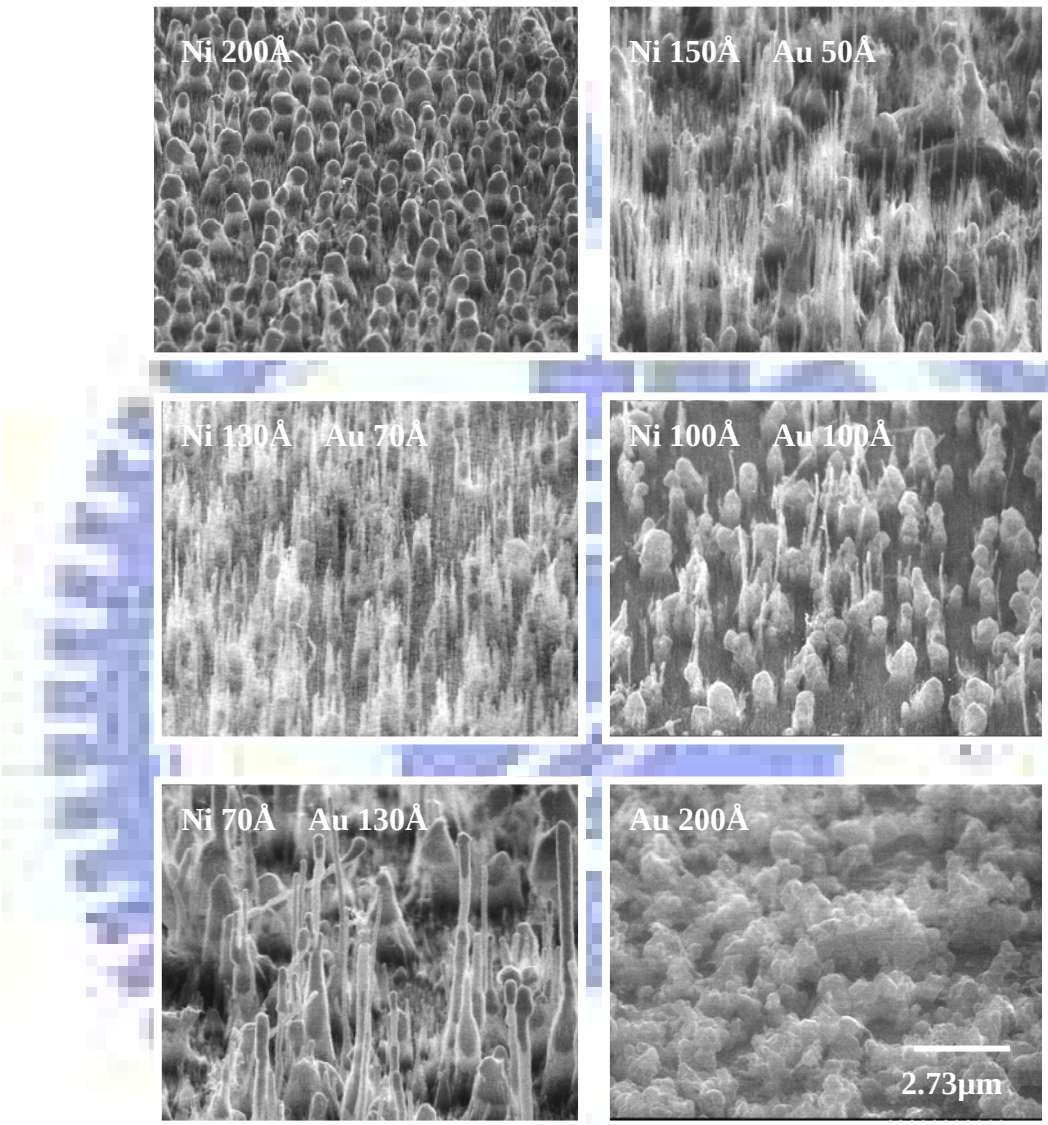

Fig. 4.12 Growth of CNTs with different density

CH_4 10 sccm H_2 40 sccm 400W -150V 10min 15torr

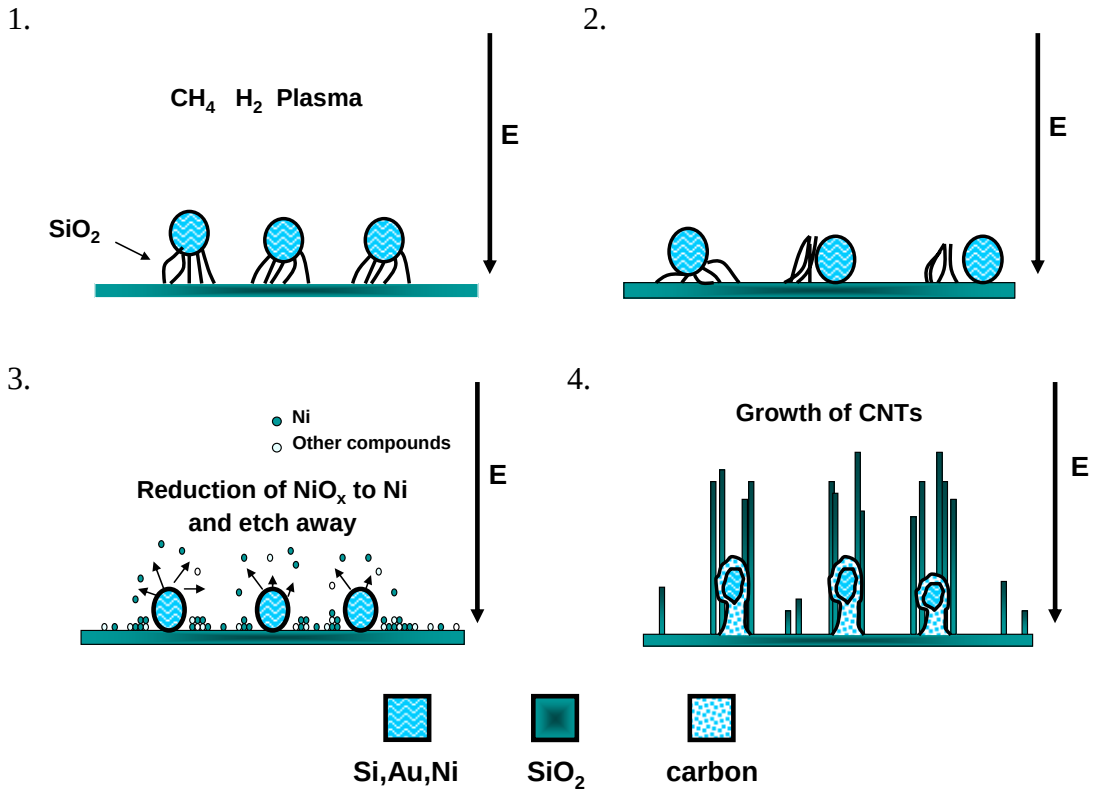

Fig. 4.13 The growth steps of density-reduced carbon nanotubes

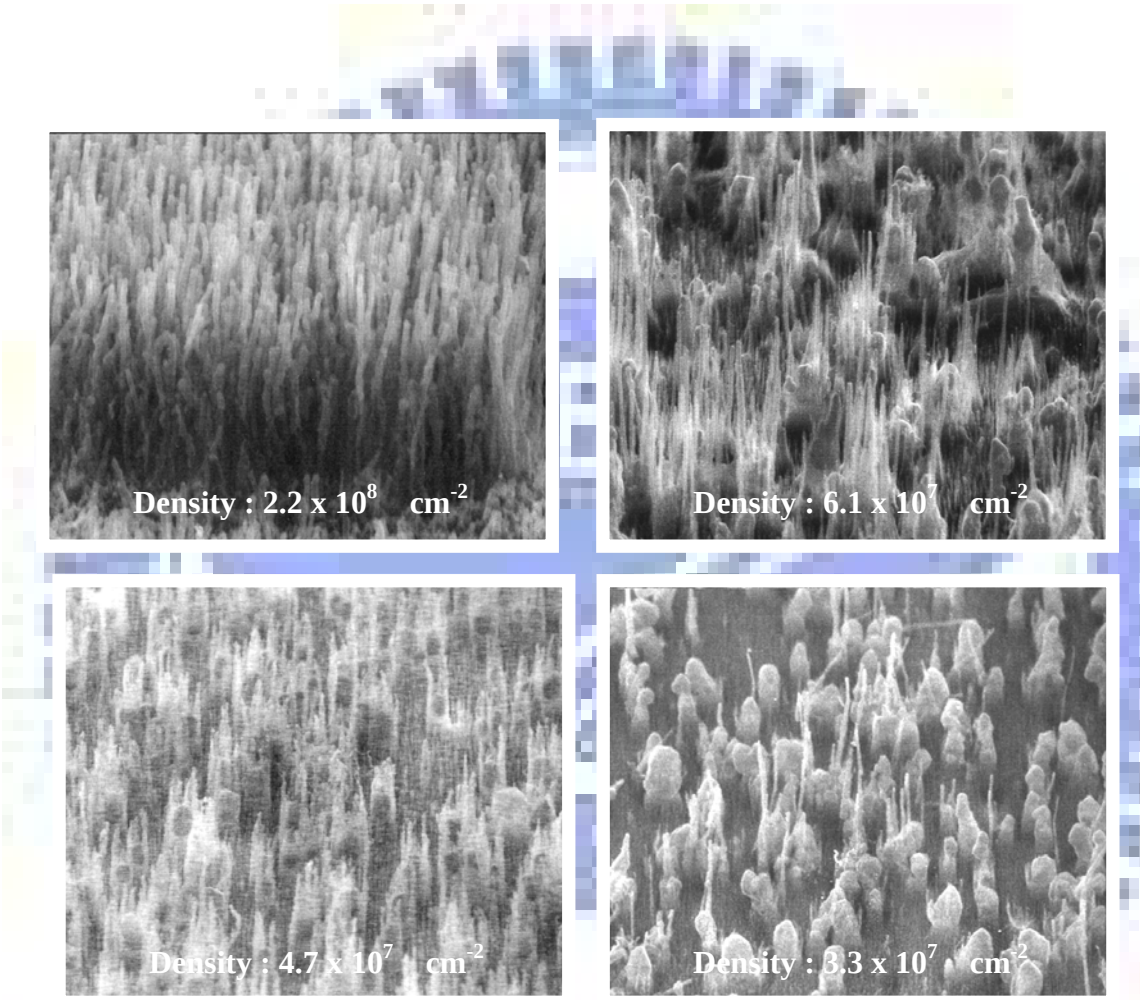

Fig. 4.14 Emission samples with different density

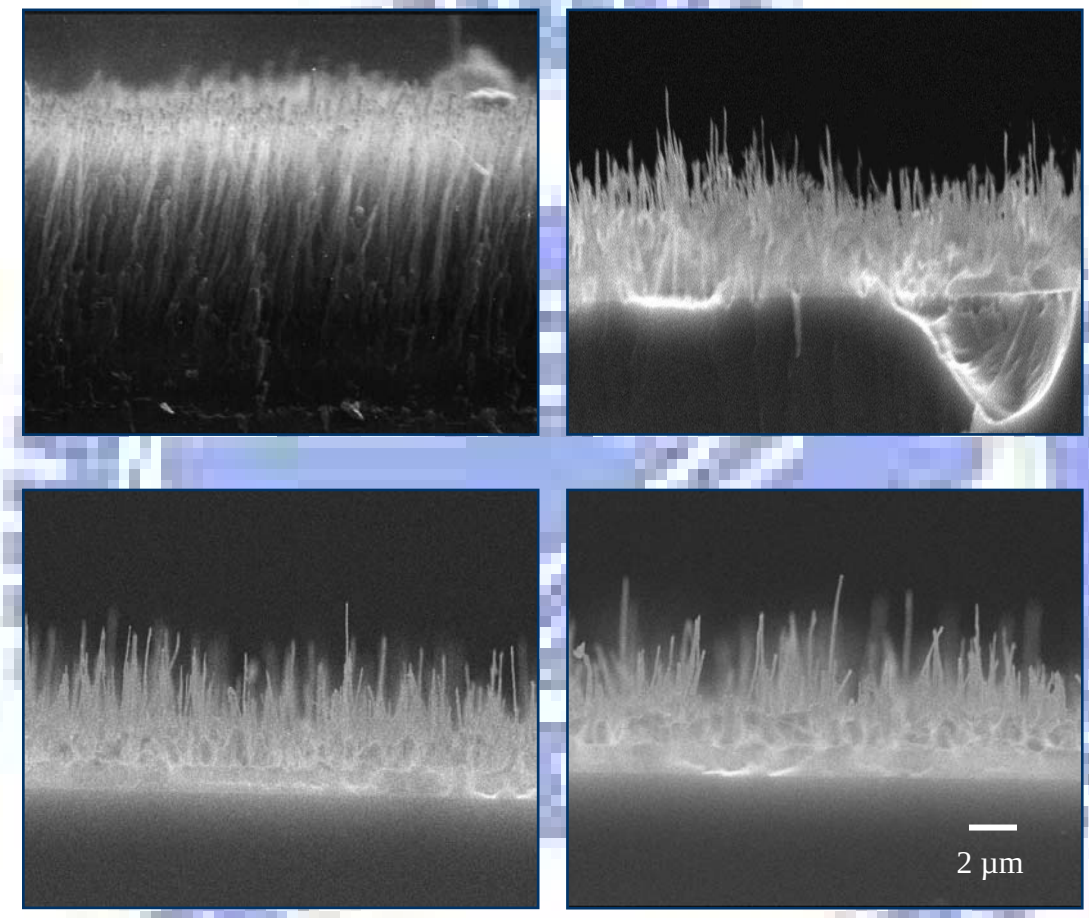

Fig. 4.15 Cross-section image of the emission samples

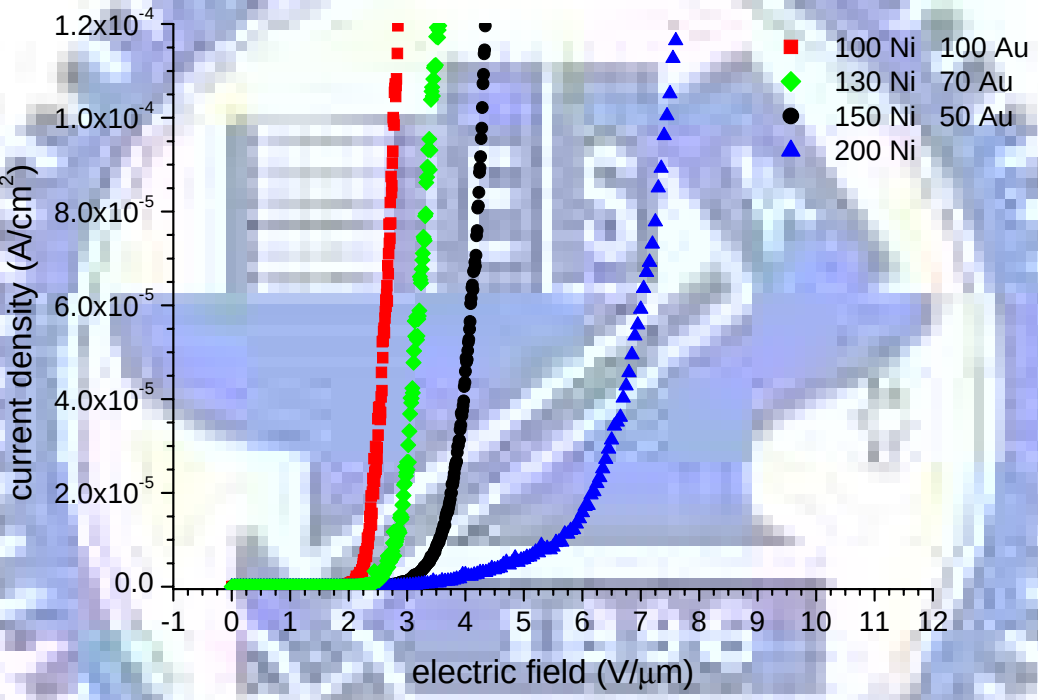

Fig. 4.16 Field emission measurement I-V plot

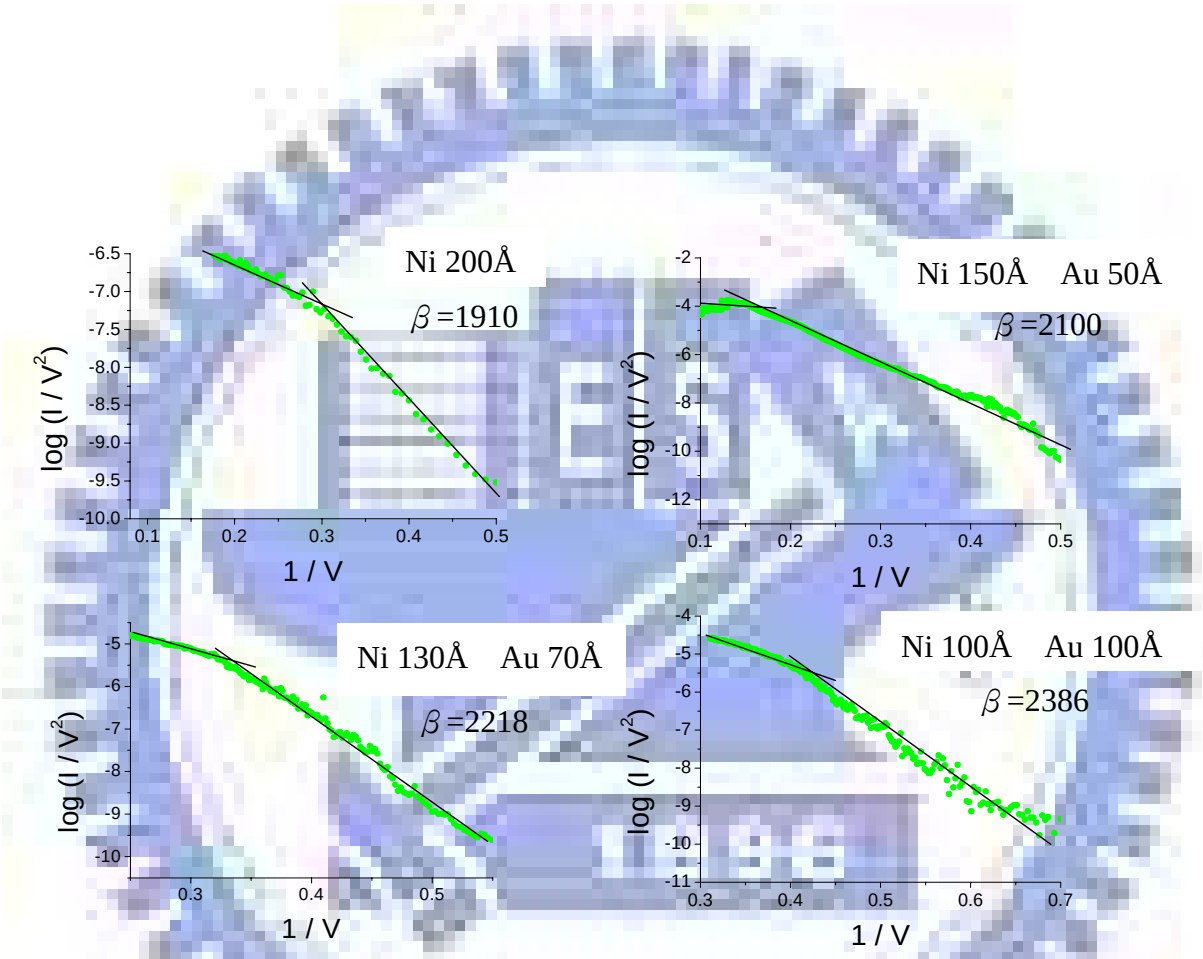

Fig. 4.17 Fowler-Nordheim plot translated from I-V measurement

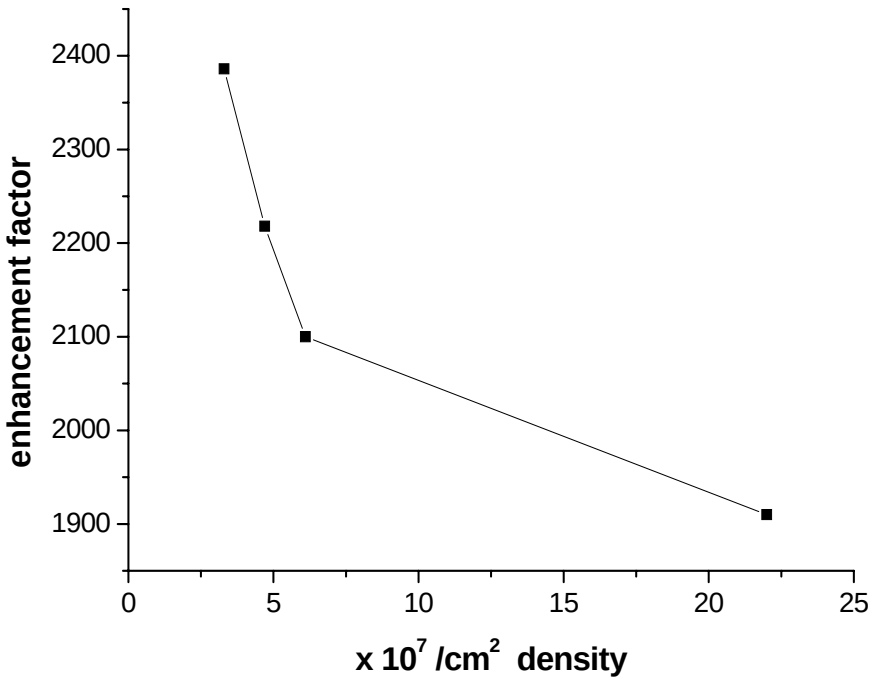

Fig. 4.18 Plot drawn by enhancement factor versus carbon nanotube density